quantum reports

Tracked for Impact Factor

CITESCORE 3.3

Article

Thermodynamic and Magnetic Properties of Weakly Interacting Electron Gas Localized in a CdSe Cylindrical Core–Shell Quantum Dot

Levon Tadevosyan, Hayk Ghaltaghchyan, Yevgeni Mamasakhlisov and Hayk Sarkisyan

MDPI

https://doi.org/10.3390/quantum7010013

quantum reports

MDPI

Article

Thermodynamic and Magnetic Properties of Weakly Interacting Electron Gas Localized in a CdSe Cylindrical Core–Shell Quantum Dot

Levon Tadevosyan [1], Hayk Ghaltaghchyan [2], Yevgeni Mamasakhlisov [2,3] and Hayk Sarkisyan [2,*]

[1] Russian-Armenian University, 123 H. Emin St., Yerevan 0015, Armenia; mrvosyan@gmail.com
[2] Institute of Applied Problems of Physics, Yerevan 0014, Armenia; haykgh@hotmail.com (H.G.); y.mamasakhlisov@ysu.am (Y.M.)
[3] Department of Molecular Physics, Yerevan State University, Yerevan 0025, Armenia
* Correspondence: hayk.sarkisyan@rau.am; Tel.: +374-95-522-782

Abstract: The thermodynamic and magnetic properties of weakly interacting electron gas localized in a CdSe cylindrical core–shell quantum dot in the presence of axial magnetic field are investigated. The entropy, mean energy, and heat capacity of such a gas are determined, and its magnetic properties (magnetization and diamagnetic susceptibility) are studied. The possibilities of controlling thermodynamic parameters by changing the geometric parameters of quantum dots are shown. Calculations show that this gas has diamagnetic properties. These results provide insights into the features of physical processes occurring in thin core–shell quantum systems, which have potential applications in opto- and nanoelectronics.

Keywords: core–shell quantum dot; partition function; entropy; diamagnetism

Academic Editor: Andrei G. Lebed

Received: 8 February 2025
Revised: 6 March 2025
Accepted: 12 March 2025
Published: 17 March 2025

Citation: Tadevosyan, L.; Ghaltaghchyan, H.; Mamasakhlisov, Y.; Sarkisyan, H. Thermodynamic and Magnetic Properties of Weakly Interacting Electron Gas Localized in a CdSe Cylindrical Core–Shell Quantum Dot. *Quantum Rep.* **2025**, *7*, 13. https://doi.org/10.3390/quantum7010013

1. Introduction

The study of ring-shaped, layered axially symmetric nanostructures and 2D quantum materials is a subject of interest for specialists both from the point of view of purely applied problems and from the point of view of the fundamental issues of quantum physics [1–6]. A striking example of this is the experimental confirmation of the Aharonov–Bohm effect for bound states of an electron in ring-shaped InAs nanostructures [7] as well as for the description of new types of topological superconductors [6].

From a practical point of view, cylindrical core–shell nanolayers and ring-shaped structures and 2D quantum materials find wide application in optoelectronic devices and various sensors operating on the basis of quantum effects [6,8–11]. A remarkable property of cylindrical core–shell nanolayers compared to spherical nanolayers is the presence, in addition to the outer and inner radii of the quantum dot cross-section, of another additional geometric parameter, namely, the height of the cylindrical nanolayer. By varying the geometric parameters of the quantum dot, it is possible to implement a subband structure of energy bonds: In the case of a thin nanolayer, a family of axial quantization levels is associated with each radial quantization level, and vice versa, at small heights, a family of radial motion levels will be associated with each axial quantization level [12,13]. This nature of energy bands leads to a rich picture of optical transitions of both intraband and interband types, which creates conditions for the flexible manipulation of the optical properties of these systems [14–17].

By synthesizing these quantum dots, as shown in the articles [18,19], we can manipulate their geometric parameters, including the size, shape, and aspect ratio, which directly

influence their optical, electronic, and surface properties. While [18] explores various synthesis techniques, including colloidal synthesis, the article [19] highlights the hydrothermal and microwave-assisted synthesis methods, which offer advantages in the scalability and uniformity of QD properties. Such control enables the fine-tuning of quantum confinement effects, bandgap energies, and emission wavelengths, making them highly versatile for applications in optoelectronics, bioimaging, and quantum computing.

In addition to the optical characteristics of axially symmetric nanolayers and quantum rings, the study of the magnetic and thermodynamic parameters of such structures is of interest [20–24]. Particularly, it is important to note that the axial symmetry of the studied structures allows an analytical description of the physical properties of cylindrical nanolayers and quantum rings in the presence of a uniform magnetic field directed along the axis of symmetry. It is clear that in the presence of a magnetic field in the single-particle Schrödinger equation, the axial part of the Hamiltonian is separated, and the influence of the magnetic field is reflected in the states of the particle in the plane of the nanolayer section. In this case, if we consider a nanolayer of small thickness, then the radial quantization levels will be separated from each other significantly further than the angular quantization levels. Then, the nature of the energy levels in the quantum dot plane will again be subband when each radial quantization level is associated with a family of angular quantization levels. The angular states of particles can be successfully described within the framework of a flat rotator model with some fixed radius R_{eff}, the value of which will be determined by the point of maximum probability density of radial states. In addition to one particle, a multiparticle gas can also be localized in a core–shell cylindrical nanolayer of small thickness. If the density of such a gas is not high, then the interactions between particles can be neglected and the statistical characteristics of such a gas can be considered within the framework of the single-particle approximation. Such a model is relatively simple but allows for an accurate analytical description of the thermodynamic and magnetic parameters of the gas being studied.

In this work, the behavior of a weakly interacting electron gas in the presence of an axial magnetic field is studied for the case of a thin cylindrical core–shell nanolayer. The thermodynamic and magnetic characteristics of the system are determined.

2. Theory

Let us consider the behavior of an electron in a thin cylindrical core–shell nanolayer with an internal radius of R_1 and an external radius of R_2 (Figure 1). The conditions for the thinness of the nanolayer consider the fulfillment of the following inequality:

$$\frac{R_2 - R_1}{R_1} \ll 1 \tag{1}$$

At the initial stage of the theoretical modeling of quantum nanostructure, an important issue is to construct a realistic model of the system's confining potential under study. Various models of confining potentials have been proposed for layered and ring-shaped two-dimensional systems, considering the presence of both an internal and external boundary. When considering this issue, the symmetry of the quantum dot under study plays a remarkable role. Thus, if in the case of a spherical core–shell quantum dot, the system has a central symmetry and is characterized by two geometric parameters, R_2—the outer radius and R_1—the inner radius, then, to describe a cylindrical core–shell quantum dot, it is necessary to take into account that the system has axial symmetry and is characterized by three geometric parameters: R_1 and R_2, the inner and outer radii, as well as the height of the cylindrical nanolayer L.

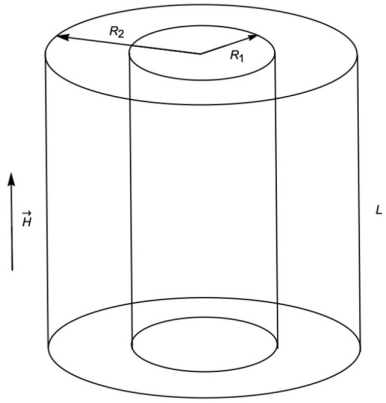

Figure 1. Schematic diagram of a thin core–shell cylindrical nanolayer.

The radial motion of particles in a cylindrical core–shell quantum dot is confined by an inner and outer boundary, and the following models have been proposed for the mathematical description of the radial confinement potential: the two-dimensional shifted oscillator model of Chakraborty–Pietilaien, radial analogue of the two-dimensional Winternitz–Smorodinsky potential, two-dimensional analogue of the Kratzer potential, and radial model of an infinitely high rectangular well with width, the rectangular stepped well [25–28].

Since this paper investigates a quantum dot of small thickness and the radial quantization is very strong, we can assume that the particles will be at the lower level of radial quantization, and the system can be considered effectively two-dimensional. For this reason, within the framework of this article, we will be satisfied with a simple model of a radial rectangular infinitely high well with a thickness of $R_2 - R_1$.

In the axial direction, one can consider the model of a one-dimensional infinitely deep well [28], the model of a parabolic well [28], the Pechy–Teller potential [29], etc. For a cylindrical CdSe core-shell quantum dots, the confinement potential is often considered as an infinitely high rectangular impermeable wall in the axial direction. The abovementioned model was used in this work. Another argument that allowed us to consider models of rectangular infinitely deep radial and axial potentials is the close connection of thin cylindrical CdSe core–shell quantum dots with CdSe nanoplatelets. As discussed in [30], experiments show that using the rectangular infinitely deep walls model for optical experiments with CdSe nanoplatelets is very successful. If we do not consider a thin cylindrical core—shell CdSe quantum dot as rolled into a tube CdSe nanoplatelet, this further supports using this model for the confinement potential.

Let us consider an electron in a cylindrical nanolayer of small thickness, in the presence of an axial magnetic field. It should be noted right away that we are considering a core/shell cylindrical quantum dot of small thickness; when we assume that the effect of radial quantization is very significant, this leads to a pronounced axial symmetry of the system under study in which the axially directed field does not violate the symmetry of the problem. Changes in the direction of the magnetic field lead to an insignificant rearrangement of the energy spectrum of the system. The presence of an axial field within the framework of this model allows us to give an exact analytical solution to the single-particle Schrödinger equation. When a magnetic field is applied at an angle to the Oz axis of a cylindrical core/shell quantum dot, it significantly complicates the mathematical description of single-electron states, and the solution of the corresponding Schrödinger equation requires a separate and comprehensive consideration. At the same time, we can say purely qualitatively that the presence of a planar component of the magnetic field can significantly modify the energy spectrum of single-electron states since this component of the magnetic

field will rearrange the spectrum of axial states of the electron. This circumstance will affect both the thermodynamic and magnetic properties of the gas under study. We approximate the confining potential of the nanolayer within the framework of the impenetrable wall model.

$$V_{conf}(\rho, z) = {V_{conf}}^{(1)}(\rho) + {V_{conf}}^{(2)}(z), \tag{2}$$

where

$${V_{conf}}^{(1)}(\rho) = \begin{cases} 0, R_1 \le \rho \le R_2 \\ \infty,\ \rho < R_1\ ,\ \rho > R_2 \end{cases}, \tag{3}$$

$${V_{conf}}^{(1)}(z) = \begin{cases} 0, |z| \le \frac{L}{2} \\ \infty, |z| > \frac{L}{2} \end{cases}, \tag{4}$$

The dimensional quantization in the radial direction is very strong, because of which the character of the electron energy levels in the plane perpendicular to the $\boldsymbol{Oz}$ axis will have the form of subbands. Each level of radial quantization will be associated with a family of angular states. From the above-mentioned equation, it follows that to describe the states of the electron, we can use the model of a flat two-dimensional rotator in a magnetic field. Then, the Hamiltonian of the system can be represented as follows:

$$\hat{H} = \frac{1}{2\mu}\left(\hat{\vec{p}} - \frac{e}{c}\vec{A}\right)^2 + {V_{conf}}^{(1)}(\rho) + {V_{conf}}^{(2)}(z), \tag{5}$$

where $\vec{A} = \left\{\boldsymbol{A_\rho} = \boldsymbol{A_z} = 0, \boldsymbol{A_\varphi} = \frac{\boldsymbol{B\rho}}{2}\right\}$ and $\boldsymbol{\mu}$ is the effective mass of the electron. In the axial direction, the electron moves in a one-dimensional infinitely deep well. For the axial wave functions and the electron energy, we can write

$$\chi_{n_z}(z) = \sqrt{\frac{2}{L}}\sin\left(\frac{\pi n_z}{L}z + \delta_{n_z}\right), \tag{6}$$

$$E_{n_z} = \frac{\pi^2\hbar^2 {n_z}^2}{2\mu L^2}, \tag{7}$$

where δ_{n_z} is the initial phase, for even states $\delta_{n_z} = \frac{\pi}{2}$, while for odd states, $\delta_{n_z} = 0$, n_z—axial quantum number. For the radial part of the Schrödinger equation, we will assume that the particle is at the ground level of radial quantization. Then, within the framework of the flat rotator model, we can assume that the electron rotates in a magnetic field with an effective radius $R_{eff} = \frac{R_1+R_2}{2}$. The corresponding Schrödinger equation for the angular part will have the following form:

$$\frac{\hbar^2}{2\mu {R_{eff}}^2}\frac{d^2\Phi}{d\varphi^2} + \frac{eB}{2\mu c}\frac{d\Phi}{d\varphi} + \frac{e^2B^2{R_{eff}}^2}{8\mu c^2}\Phi = E_{rot}\Phi, \tag{8}$$

Considering the symmetry of the problem, as well as the periodicity condition of the angular wave function $\Phi(\varphi + 2\pi) = \Phi(\varphi)$ for $\Phi(\varphi)$, we can write

$$\Phi(\varphi) = \Phi_m(\varphi) = \frac{1}{\sqrt{2\pi}}e^{im\varphi}, \tag{9}$$

where $m = 0; \pm 1; \pm 2$ is the magnetic quantum number. Substituting expression (9) into the Schrödinger Equation (8) for the energy $E_{rot} \equiv E_m$, we obtain

$$E_m = \frac{\hbar^2}{2\mu {R_{eff}}^2}\left(m - \frac{\mathcal{F}}{\mathcal{F}_0}\right)^2, \tag{10}$$

where $\mathcal{F} = B\pi R^2$ is the magnetic field flux through a circle of radius R_{eff}, and $\mathcal{F}_0 = 2\pi\frac{\hbar c}{e}$ is the magnetic flux quantum. Thus, for the total energy of an electron, measured from the first level of radial quantization, we can write

$$E_{m,n_z} = \frac{\pi^2\hbar^2 {n_z}^2}{2\mu L^2} + \frac{\hbar^2}{2\mu {R_{eff}}^2}\left(m - \frac{\mathcal{F}}{\mathcal{F}_0}\right)^2. \tag{11}$$

Now, let us assume that the nanolayer under consideration contains a weakly interacting electron gas. Our goal will be to study the thermodynamic and magnetic characteristics of such a gas within the framework of Boltzmann statistics. In this approximation, we have the following expression for the partition function $Z = \frac{1}{N!}[Z_0]^N$, where

$$Z_0 = \sum_{m=-\infty}^{+\infty}\sum_{n_z=1}^{\infty} e^{-\beta(E_m + E_{n_z})}, \tag{12}$$

while $\beta = \frac{1}{KT}$. Let us proceed to the calculation of the specified partition function. In the axial direction, we have a sum of the following type:

$$S_1 = \sum_{n_z=1}^{\infty} e^{-\beta\frac{\pi^2\hbar^2 {n_z}^2}{2\mu L^2}}, \tag{13}$$

If we introduce the notation $\gamma_1 = \beta\frac{\pi\hbar^2}{2\mu L^2}$, then, taking into account the definition of Ramanujan's theta function $\varphi(q) = \sum_{n=-\infty}^{+\infty} q^{n^2}$, for S_1, we will have

$$S_1 = \sum_{n_z=1}^{\infty} e^{-\gamma_1\pi {n_z}^2} = \frac{\varphi(e^{-\gamma_1\pi}) - 1}{2}, \tag{14}$$

Note that $\varphi(q)$ also has an integral representation of the following form:

$$\varphi(q) = 1 + \int_0^{\infty} \frac{e^{-\frac{1}{2}t^2}}{\sqrt{2\pi}}\left[\frac{4q\left(1 - \cosh\left(\sqrt{2\log q}t\right)\right)}{q^4 - 2q^2\cosh\left(\sqrt{2\log q}t\right) + 1}\right]dt, \tag{15}$$

where q, with the consideration of the Equation (16), is defined as $q = e^{-\gamma_1\pi}$. Let us turn to the second sum in the expression for Z_0:

$$S_2 = \sum_{m=-\infty}^{+\infty} e^{-\pi\gamma_2\left[m - \frac{\mathcal{F}}{\mathcal{F}_0}\right]^2}, \tag{16}$$

where $\gamma_2 = \beta\frac{\hbar^2}{2\pi\mu {R_{eff}}^2}$. Let us note that for S_2, we can write the following:

$$S_2 = e^{-\pi\gamma_2\left(\frac{\mathcal{F}}{\mathcal{F}_0}\right)^2} + \sum_{m=1}^{+\infty} e^{-\pi\gamma_2\left[m - \frac{\mathcal{F}}{\mathcal{F}_0}\right]^2} + \sum_{m=1}^{+\infty} e^{-\pi\gamma_2\left[m + \frac{\mathcal{F}}{\mathcal{F}_0}\right]^2}, \tag{17}$$

We can represent the first sum in Equation (18) in the following form:

$${S_2}' = \sum_{m=1}^{+\infty} e^{-\pi\gamma_2\left[m - \frac{\mathcal{F}}{\mathcal{F}_0}\right]^2} = \sum_{m=1}^{m'} e^{-\pi\gamma_2\left[m - \frac{\mathcal{F}}{\mathcal{F}_0}\right]^2} + \sum_{m=m'+1}^{\infty} e^{-\pi\gamma_2\left[m - \frac{\mathcal{F}}{\mathcal{F}_0}\right]^2}, \tag{18}$$

In Equation (19), we are considering that $m' \gg \frac{\mathcal{F}}{\mathcal{F}_0}$, and starting from $m' + 1$, the following approximate equality takes place:

$$m - \frac{\mathcal{F}}{\mathcal{F}_0} \approx m, \tag{19}$$

Adding and subtracting the sum to the right side of Equation (19), we can obtain

$$\sum_{m=1}^{m'} e^{-\pi\gamma_2 m^2}, \tag{20}$$

for $S_2{}'$, we will have

$$S_2{}' = \sum_{m=1}^{m'} e^{-\pi\gamma_2[m-\frac{\mathcal{F}}{\mathcal{F}_0}]^2} - \sum_{m=1}^{m'} e^{-\pi\gamma_2 m^2} + \sum_{m=1}^{\infty} e^{-\pi\gamma_2 m^2}. \quad (21)$$

Let us introduce the following notations:

$$K^-(m') = \sum_{m=1}^{m'} e^{-\pi\gamma_2[m-\frac{\mathcal{F}}{\mathcal{F}_0}]^2}, \quad (22)$$

$$K(m') = \sum_{m=1}^{m'} e^{-\pi\gamma_2 m^2}, \quad (23)$$

and considering the form of Ramanujan's theta function, for $S_2{}'$, we finally find

$$S_2{}' = K^-\left(m'\right) - K\left(m'\right) + \frac{\varphi(e^{-\gamma_2\pi}) - 1}{2}, \quad (24)$$

Similarly, for the second sum $S_2{}''$ in Equation (17), we obtain

$$S_2{}'' = \sum_{m=1}^{+\infty} e^{-\pi\gamma_2[m+\frac{\mathcal{F}}{\mathcal{F}_0}]^2} \approx K^+\left(m'\right) - K\left(m'\right) + \frac{\varphi(e^{-\gamma_2\pi}) - 1}{2}, \quad (25)$$

where $K^+\left(m'\right) = \sum_{m=1}^{m'} e^{-\pi\gamma_2[m+\frac{\mathcal{F}}{\mathcal{F}_0}]^2}$. Based on the above results for Z_0, we can finally write

$$Z_0 = \left\{K^+\left(m'\right) + K^-\left(m'\right) - 2K\left(m'\right) + \varphi\left(e^{-\gamma_2\pi}\right) - 1 + e^{-\pi\gamma_2(\frac{\mathcal{F}}{\mathcal{F}_0})^2}\right\} \times \left\{\frac{\varphi(e^{-\gamma_1\pi}) - 1}{2}\right\}, \quad (26)$$

Considering the equality that we introduced for the partition function, we have the following relationship:

$$Z = \frac{1}{N!}\{K^+(m') + K^-(m') - 2K(m') + \varphi\left(e^{-\gamma_2\pi}\right) - 1 + e^{-\pi\gamma_2(\frac{\mathcal{F}}{\mathcal{F}_0})^2}\}^N \times \left\{\frac{\varphi(e^{-\pi\gamma_1}) - 1}{2}\right\}^N. \quad (27)$$

Having the expression for Z, we can proceed to the calculation of the thermodynamic and magnetic parameters of the given gas:

Heat Capacity:

$$C_v = -\frac{1}{kT^2}\frac{\partial^2 Z(N)}{\partial(kT)^{-2}}, \quad (28)$$

Entropy:

$$S = \frac{\partial}{\partial T}(kTlnZ(N)), \quad (29)$$

Magnetization:

$$M = \frac{kT}{Z(N)}\frac{\partial Z(N)}{\partial H}, \quad (30)$$

Magnetic Susceptibility:

$$\chi = \frac{\partial\langle M\rangle}{\partial H}, \quad (31)$$

3. Discussion

Based on the data obtained, it is possible to calculate the thermodynamic parameters of a given gas. Below, you can find the calculation for the mean energy $< E >$, entropy S, heat capacity C_V, magnetization M, and magnetic susceptibility χ. Calculations are performed for the CdSe cylindrical core–shell quantum dot with the parameters presented in Table 1. R_{eff} changes in the following range: $1.9 < R_{eff} < 2.1$. CdSe structures, whether core–shell quantum dots or nanoplatelets, are among the most effectively implemented by

various synthesis methods [30,31]. The material parameters of these systems have been well studied, and various geometric models have been constructed to describe the states of electrons, impurities, and excitons in such structures [32,33]. Basic knowledge of the band structure of CdSe core–shell quantum dots or nanoplatelets allows one to study in detail the various physical characteristics of such systems, in particular, intraband and interband optical transitions. At the same time, as calculations show, exciton states can significantly affect the nature of optical transitions. Meanwhile, the band gap in the case of CdSe is relatively large, unlike that of PbS, which allows for the implementation of optical sensors that operate in higher frequency ranges [34].

Table 1. Parameters of considered material. These parameters are taken from [34]. Some of these data points interpolated using available data.

Parameter	CdSe
d_0, nm	0.3
$m^e_\perp$, m_0	0.144 (4.5 ML)
	0.138 (5.5 ML)
	0.13 (7.5 ML)
$m^{hh}_\perp$, m_0	0.92 (4.5 ML)
	0.9 (5.5 ML)
	0.88 (7.5 ML)
$\mu_\parallel$, m_0	0.09 (4.5 ML)
	0.081 (5.5 ML)
	0.076 (7.5 ML)
E_g, eV	2.15 (4.5 ML)
	2.0 (5.5 ML)
	1.76 (7.5 ML)

Figure 2 shows the dependency of the mean energy of the gas under study on the R_{eff} at different temperatures. As expected, with increasing temperature, the average energy of the gas increases. At the same time, with the growth of the effective radius, the distance between the levels of angular motion decreases and the electron gas at a higher temperature is more sensitive to changes in the geometric parameters of the quantum dot, because of which the graph of the dependence $< E > \left(R_{eff}\right)$ corresponding to a higher temperature undergoes more significant changes. The latter circumstances are a direct consequence of the quantum nature of the energy spectrum of the particle.

Figure 3 shows the dependency of the entropy of the gas under study on the R_{eff} at different temperatures. For higher temperature, the corresponding curve of dependence is higher. On the other hand, as it was stated above, with increase in R_{eff}, the distance between energy levels decreases, which leads to an increase in number of states on the unit energy segment. This, in turn, leads to increase in entropy of gas. The abovementioned relationship is shown by numerical calculations.

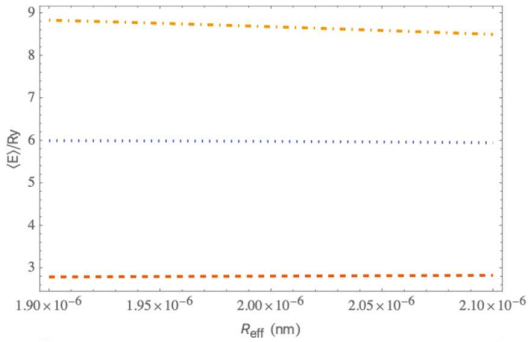

Figure 2. The dependency of the mean energy of the electron gas on the R_{eff} at different temperatures, where Y-axis values are relative to the Rydberg energy and the values of X-axis values are in nanometers. Dashed red line corresponds to the temperature $T = 100$ K, dotted blue line corresponds to $T = 200$ K, and dot–dash orange line corresponds to $T = 300$ K.

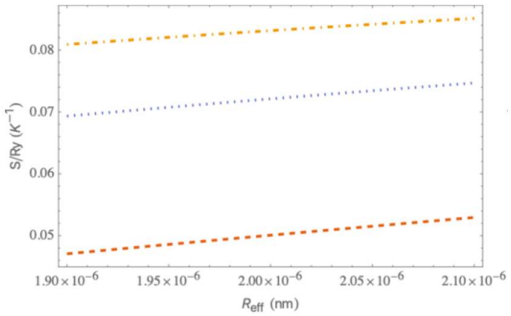

Figure 3. The dependency of the entropy of the electron gas on the R_{eff} at different temperatures, where Y-axis values are relative to the Rydberg energy and the values of X-axis values are in nanometers. Dashed red line corresponds to the temperature $T = 100$K, dotted blue line corresponds to $T = 200$K, and dot–dash orange line corresponds to $T = 300$K.

Figure 4 shows the dependency of the heat capacity of the gas under study on the R_{eff} at different temperatures. As the temperature increases, the heat capacity decreases, since at a higher temperature, in the process of heat transfer, electrons more easily move to higher levels. Similarly, with an increase in R_{eff}, due to a decrease in the distance between levels, electrons also more easily move to higher excited levels.

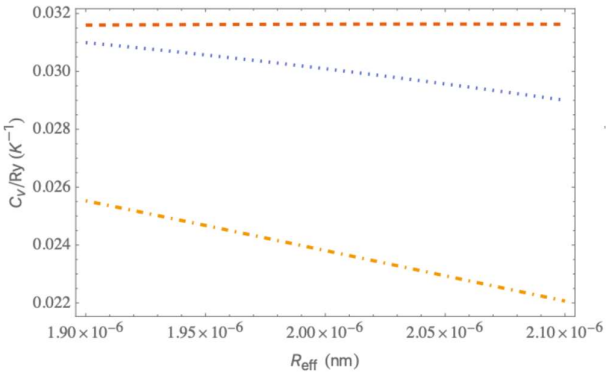

Figure 4. The dependency of the heat capacity of the electron gas on the R_{eff} at different temperatures, where Y-axis values are relative to the Rydberg energy and the values of X-axis values are in nanometers. Dashed red line corresponds to the temperature $T = 100$K, dotted blue line corresponds to $T = 200$K, and dot–dash orange line corresponds to $T = 300$K.

With the growth of the magnetic field, the current caused by the rotation of the electron on the surface of the nanolayer increases; this follows from the expression for the quantum current of a spinless particle in a magnetic field:

$$\vec{j} = \frac{ie\hbar}{2\mu}(\psi\overline{\nabla}\psi^* - \psi^*\overline{\nabla}\psi) - \frac{e^2}{\mu c}\vec{A}|\psi|^2. \quad (32)$$

Thus, with the growth in H, the current will grow, and consequently, the electron magnetic moment p_m will also grow. This leads to an increase in the magnetization of the system in modulus.

On the other hand, an increase in the temperature leads to an increase in the orbital current of the electron on the surface of the nanolayer. Considering the abovementioned relationship, we obtain the dependences $M(H)$ at different temperatures, shown in Figure 5. It should be noted that the dependences are linear; consequently, the diamagnetic susceptibility χ practically does not change with increasing H. However, a higher temperature will correspond to a larger value in modulus of χ (Figure 6).

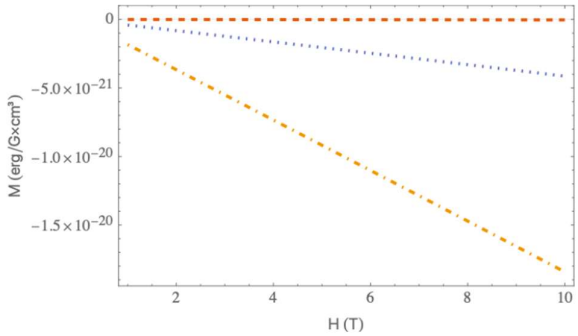

Figure 5. The dependency of the magnetization of the electron gas on the magnetic field at different temperatures, where the values of X-axis are in teslas. Dashed red line corresponds to the temperature $T = 100$K, dotted blue line corresponds to $T = 200$K, and dot–dash orange line corresponds to $T = 300$K.

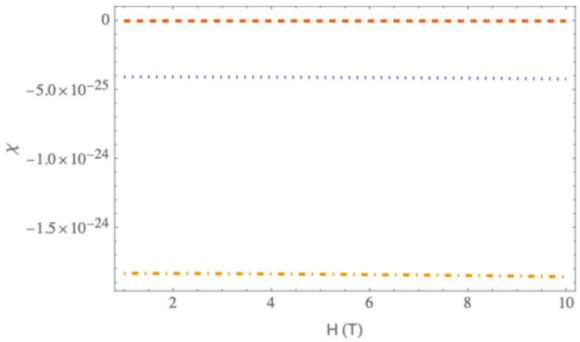

Figure 6. The dependency of the magnetic susceptibility of the electron gas on the magnetic field strength at different temperatures, where the values of X-axis are in teslas. Dashed red line corresponds to the temperature $T = 100$K, dotted blue line corresponds to $T = 200$K, and dot–dash orange line corresponds to $T = 300$K.

In addition to the thermodynamic properties, studying the optical and transport characteristics of low-dimensional structures provides valuable insights into the physical processes occurring within them. Notably, in [35,36], both theoretical and experimental research on the optical and magneto-optical characteristics of two-dimensional and quasi-two-dimensional systems demonstrated the feasibility of implementing the generalized Kohn theorem in electron and hole subsystems.

Beyond magneto-optical effects, magneto-transport phenomena in low-dimensional structures are also of significant interest. This topic is explored in [37–40], where it was shown that the electronic and transport properties of these systems are highly sensitive to factors such as material composition, quantum confinement, and magnetic interactions. Studies have demonstrated that anisotropic behavior, doping effects, and the interplay between electronic states and external fields play a crucial role in shaping the magneto-transport characteristics of low-dimensional materials. These findings highlight the complex and tunable nature of transport phenomena, offering new possibilities for advanced electronic and spintronic applications.

Thus, the study of thermodynamic characteristics, along with the optical and kinetic properties, is an effective tool that allows us to identify the behavioral features of multiparticle systems within low-dimensional structures.

4. Conclusions

Thus, in this work we have determined the thermodynamic and magnetic characteristics of a weakly interacting electron gas in a thin cylindrical CdSe nanolayer in the presence of an axial magnetic field. Calculations show that with an increase in the temperature and R_{eff} of the core–shell quantum dot, the mean energy and entropy of the electron gas increases. On the other hand, the heat capacity of the gas decreases with an increase in temperature and effective radius. The magnetization of the electron gas increases with an increase in the magnetic field and temperature. It important to note that the electron gas has a pronounced diamagnetism. It is noteworthy that the relationship between magnetization and the value of the magnetic field is almost linear, as a result of which, the value of diamagnetic susceptibility practically does not change.

Our results are tightly connected with those of previous works on CdSe-based quantum dots and nanoplatelets. The article [31] demonstrated the synthesis and characterization of (CdSe)ZnS core–shell quantum dots, revealing how quantum confinement and passivation influence optical properties such as photoluminescence efficiency, and excitonic transitions. Additionally, the article [30] investigated exciton dynamics in CdSe nanoplatelets, highlighting the impact of lateral quantum confinement on optical absorption and energy level quantization. The correlation between these effects and weakly interacting electron gases in core–shell quantum dots remains an open question, yet our results suggest that the thermodynamic and magnetic properties could be experimentally observed through techniques like magneto-optical spectroscopy, temperature-dependent photoluminescence, and calorimetry. These insights could contribute to the development of tunable quantum dot-based devices for optoelectronics and spintronics (QD-LEDs, spin-QD transistors, solar cells, etc.) [41,42].

Author Contributions: Conceptualization, H.S., H.G. and Y.M.; methodology, H.S., Y.M. and L.T.; formal analysis, H.G. and L.T.; writing—original draft preparation, H.S. and L.T.; writing—review and editing, H.S., H.G., Y.M. and L.T.; supervision, H.S. All authors have read and agreed to the published version of the manuscript.

Funding: The work was funded by RA Science Committee as part of the "Leading scientific research support program" in the framework of research project 21AG-1C022.

Data Availability Statement: No new data were created or analyzed in this study. Data sharing is not applicable to this article.

Conflicts of Interest: The authors declare no conflicts of interest of the manuscript. The funders had no role in the design of the study; in the collection, analyses, or interpretation of data; in the writing of the manuscript; or in the decision to publish the results.

References

1. Wu, J.; Wang, Z.M.; Dorogan, V.G.; Li, S.; Zhou, Z.; Li, H.; Lee, J.; Kim, E.S.; Mazur, Y.I.; Salamo, G.J. Strain-Free Ring-Shaped Nanostructures by Droplet Epitaxy for Photovoltaic Application. *Appl. Phys. Lett.* **2012**, *101*, 043904. [CrossRef]
2. Lee, J.H.; Wang, Z.M.; Ware, M.E.; Wijesundara, K.C.; Garrido, M.; Stinaff, E.A.; Salamo, G.J. Super Low Density InGaAs Semiconductor Ring-Shaped Nanostructures. *Cryst. Growth Des.* **2008**, *8*, 1945–1951. [CrossRef]
3. Rafiee, E.; Negahdari, R. Cancer Cell Detection Biosensor Based on Graphene-Plasmonic Split Square-Ring-Shaped Nanostructure. *Plasmonics* **2023**, *18*, 431–440. [CrossRef]
4. Cui, W.; Li, L.; He, Z.; He, H.; He, X.; Xia, B.; Zhong, Z.; Song, C.; Li, L.; Xue, W.; et al. Enhanced Plasmonic Field and Focusing for Ring-Shaped Nanostructures via Radial Vector Beam. *Results Phys.* **2021**, *26*, 104412. [CrossRef]
5. Movilla, J.L.; Climente, J.I.; Planelles, J. Dielectric Polarization in Axially-Symmetric Nanostructures: A Computational Approach. *Comput. Phys. Commun.* **2010**, *181*, 92–98. [CrossRef]
6. Karn, N.K.; Sharma, M.M.; Awana, V.P.S. Non-Trivial Band Topology in the Superconductor AuSn4: A First Principle Study. *Supercond. Sci. Technol.* **2022**, *35*, 114002. [CrossRef]
7. Lorke, A.; Luyken, R.J.; Govorov, A.O.; Kotthaus, J.P.; Garcia, J.M.; Petroff, P.M. Spectroscopy of Nanoscopic Semiconductor Rings. *Phys. Rev. Lett.* **2000**, *84*, 2223–2226. [CrossRef]
8. Harutyunyan, V.A.; Hayrapetyan, D.B.; Kazaryan, E.M. Interband Absorption and Photoluminescence in the Cylindrical Layered CdS/HgS/CdS Heterostructure. *J. Contemp. Phys.* **2018**, *53*, 48–57. [CrossRef]
9. Zeiri, N.; Baser, P.; Jahromi, H.D.; Yahyaoui, N.; Ed-Dahmouny, A.; Sfina, N.; Duque, C.A.; Said, M. Effects of the Size and Applied Electric Field on the Photoionization Cross-Section of Elliptical Cylindrical CdS/ZnS Core-Shell Quantum Dots Immersed in Various Dielectric Matrices. *Opt. Laser Technol.* **2025**, *182*, 111822. [CrossRef]
10. El-Yadri, M.; El Hamdaoui, J.; Aghoutane, N.; Pérez, L.M.; Baskoutas, S.; Laroze, D.; Díaz, P.; Feddi, E.M. Optoelectronic Properties of a Cylindrical Core/Shell Nanowire: Effect of Quantum Confinement and Magnetic Field. *Nanomaterials* **2023**, *13*, 1334. [CrossRef]
11. Harutyunyan, V.A. Electro-Optical Transitions in a Semiconductor Cylindrical Nanolayer. *Phys. Solid State* **2012**, *54*, 1096–1103. [CrossRef]
12. Harutyunyan, V.A.; Kazaryan, E.M.; Kostanyan, A.A.; Sarkisyan, H.A. Interband Transitions in Cylindrical Layer Quantum Dot: Influence of Magnetic and Electric Fields. *Phys. E Low-Dimens. Syst. Nanostructures* **2007**, *36*, 114–118. [CrossRef]
13. Aghekyan, N.G.; Kazaryan, E.M.; Petrosyan, L.S.; Sarkisyan, H.A. Two Electronic States in a Quantum Ring: Mathieu Equation Approach. *J. Phys. Conf. Ser.* **2010**, *248*, 012048. [CrossRef]
14. Harutyunyan, V.A.; Aramyan, K.S.; Petrosyan, H.S.; Demirjian, G.H. Optical Transitions in Spherical Quantized Layer under the Presence of Radial Electrical Field. *Phys. E Low-Dimens. Syst. Nanostructures* **2004**, *24*, 173–177. [CrossRef]
15. Wang, Y.; Dou, W. Interband and Intraband Transitions, as Well as Charge Mobility in Driven Two-Band Model with Electron–Phonon Coupling. *J. Chem. Phys.* **2024**, *161*, 204104. [CrossRef]
16. Harutyunyan, V.A. Semiconductor Nanocylindrical Layer in a Strong Electric Field: Spectrum of Carriers and Intraband Transitions. *Phys. Solid State* **2010**, *52*, 1744–1749. [CrossRef]
17. Ed-Dahmouny, A.; Zeiri, N.; Arraoui, R.; Es-Sbai, N.; Jaouane, M.; Fakkahi, A.; Sali, A.; El-Bakkari, K.; Duque, C.A. The Third-Order Nonlinear Optical Susceptibility in an Ellipsoidal Core-Shell Quantum Dot Embedded in Various Dielectric Surrounding Matrices. *Phys. E Low-Dimens. Syst. Nanostructures* **2023**, *153*, 115784. [CrossRef]
18. Agarwal, K.; Rai, H.; Mondal, S. Quantum Dots: An Overview of Synthesis, Properties, and Applications. *Mater. Res. Express* **2023**, *10*, 062001. [CrossRef]
19. Valizadeh, A.; Mikaeili, H.; Samiei, M.; Farkhani, S.M.; Zarghami, N.; Kouhi, M.; Akbarzadeh, A.; Davaran, S. Quantum Dots: Synthesis, Bioapplications, and Toxicity. *Nanoscale Res. Lett.* **2012**, *7*, 480. [CrossRef]
20. Maksym, P.A.; Chakraborty, T. Effect of Electron-Electron Interactions on the Magnetization of Quantum Dots. *Phys. Rev. B* **1992**, *45*, 1947–1950. [CrossRef]
21. Pietiläinen, P.; Halonen, V.; Chakraborty, T. Electron Correlations in Quantum Ring and Dot Systems. *Phys. B Condens. Matter* **1995**, *212*, 256–260. [CrossRef]
22. Lafaurie, L.G.; Suaza, Y.A.; Laroze, D.; Gutiérrez, W.; Marín, J.H. Thermodynamic Properties of an Artificial Molecule Quantum Rings: Geometric and External Field Effects. *Phys. B Condens. Matter* **2024**, *679*, 415786. [CrossRef]
23. Manninen, M.; Koskinen, M.; Reimann, S.M.; Mottelson, B. Magnetic Properties of Quantum Dots and Rings. *Eur. Phys. J. D* **2001**, *16*, 381–385. [CrossRef]
24. Chouef, S.; Hbibi, M.; Boussetta, R.; El Moussaouy, A.; Mommadi, O.; Falyouni, F.; Duque, C.A. Influence of Magnetic Field and Temperature on Thermodynamic Properties of Curved Two-Low-Dimensional Nanostructures: Presence of Shallow Donor Impurity. *J. Magn. Magn. Mater.* **2025**, *614*, 172729. [CrossRef]
25. Chakraborty, T.; Pietiläinen, P. Electron-Electron Interaction and the Persistent Current in a Quantum Ring. *Phys. Rev. B* **1994**, *50*, 8460–8468. [CrossRef]

26. Tan, W.-C.; Inkson, J.C. Electron States in a Two-Dimensional Ring—An Exactly Soluble Model. *Semicond. Sci. Technol.* **1996**, *11*, 1635–1641. [CrossRef]
27. Bandos, T.V.; Cantarero, A.; García-Cristóbal, A. Finite Size Effects on the Optical Transitions in Quantum Rings under a Magnetic Field. *Eur. Phys. J. B* **2006**, *53*, 99–108. [CrossRef]
28. Flügge, S. *Practical Quantum Mechanics*; Springer: Berlin/Heidelberg, Germany, 1971; ISBN 978-3-540-65035-5.
29. Pöschl, G.; Teller, E. Bemerkungen zur Quantenmechanik des anharmonischen Oszillators. *Z. Phys.* **1933**, *83*, 143–151. [CrossRef]
30. Failla, M.; García Flórez, F.; Salzmann, B.B.V.; Vanmaekelbergh, D.; Stoof, H.T.C.; Siebbeles, L.D.A. Observation of the Quantized Motion of Excitons in CdSe Nanoplatelets. *Phys. Rev. B* **2020**, *102*, 195405. [CrossRef]
31. Dabbousi, B.O.; Rodriguez-Viejo, J.; Mikulec, F.V.; Heine, J.R.; Mattoussi, H.; Ober, R.; Jensen, K.F.; Bawendi, M.G. (CdSe)ZnS Core–Shell Quantum Dots: Synthesis and Characterization of a Size Series of Highly Luminescent Nanocrystallites. *J. Phys. Chem. B* **1997**, *101*, 9463–9475. [CrossRef]
32. Hbibi, M.; Mommadi, O.; Chouef, S.; Boussetta, R.; Belamkadem, L.; Moussaouy, A.E.; Falyouni, F.; Duque, C.M.; Vinasco, J.A.; Duque, C.A. Finite Confinement Potentials, Core and Shell Size Effects on Excitonic and Electron-Atom Properties in Cylindrical Core/Shell/Shell Quantum Dots. *Sci. Rep.* **2022**, *12*, 14854. [CrossRef] [PubMed]
33. Pulgar-Velásquez, L.; Sierra-Ortega, J.; Vinasco, J.A.; Laroze, D.; Radu, A.; Kasapoglu, E.; Restrepo, R.L.; Gil-Corrales, J.A.; Morales, A.L.; Duque, C.A. Shallow Donor Impurity States with Excitonic Contribution in GaAs/AlGaAs and CdTe/CdSe Truncated Conical Quantum Dots under Applied Magnetic Field. *Nanomaterials* **2021**, *11*, 2832. [CrossRef] [PubMed]
34. Baghdasaryan, D.A.; Harutyunyan, V.A.; Hayrapetyan, D.B.; Kazaryan, E.M.; Baskoutas, S.; Sarkisyan, H.A. Exciton States and.Optical Absorption in CdSe and PbS Nanoplatelets. *Nanomaterials* **2022**, *12*, 3690. [CrossRef]
35. Ustimenko, R.V.; Vinnichenko, M.Y.; Karaulov, D.A.; Sarkisyan, H.A.; Hayrapetyan, D.B.; Firsov, D.A. Effect of Doping and Interband Pumping on the Optical Properties of GeSi/Si Quantum Dot Nanostructures for Infrared Detectors. *ACS Appl. Nano Mater.* **2024**, *7*, 27245–27253. [CrossRef]
36. Brey, L.; Johnson, N.F.; Halperin, B.I. Optical and Magneto-Optical Absorption in Parabolic Quantum Wells. *Phys. Rev. B* **1989**, *40*, 10647–10649. [CrossRef]
37. Karn, N.K.; Sharma, M.M.; Felner, I.; Awana, V.P.S. Anisotropy in Electronic and Magneto-Transport of 2D Superconductor NbSe2. *J. Supercond. Nov. Magn.* **2024**, *37*, 1381–1391. [CrossRef]
38. Kumar, K.; Awana, V.P.S. Exploration of Magneto-Transport Properties of $Mn_xSb_{2-x}Te_3$(x = 0.0,0.1) Topological Insulator. *Mater. Today Proc.* **2023**. [CrossRef]
39. Takeuchi, Y.; Sepehri-Amin, H.; Sugimoto, S.; Hiroto, T.; Kasai, S. Magnetic and Magneto-Transport Properties of Non-Collinear Antiferromagnetic Mn3Ge Epitaxial Films. *APL Mater.* **2024**, *12*, 071110. [CrossRef]
40. Paravicini-Bagliani, G.L.; Appugliese, F.; Richter, E.; Valmorra, F.; Keller, J.; Beck, M.; Bartolo, N.; Rössler, C.; Ihn, T.; Ensslin, K.; et al. Magneto-Transport Controlled by Landau Polariton States. *Nat. Phys.* **2019**, *15*, 186–190. [CrossRef]
41. Sapienza, L.; Al-Khuzheyri, R.; Dada, A.; Griffiths, A.; Clarke, E.; Gerardot, B.D. Magneto-Optical Spectroscopy of Single Charge-Tunable InAs/GaAs Quantum Dots Emitting at Telecom Wavelengths. *Phys. Rev. B* **2016**, *93*, 155301. [CrossRef]
42. Calvin, J.J.; Brewer, A.S.; Crook, M.F.; Kaufman, T.M.; Alivisatos, A.P. Observation of Negative Surface and Interface Energies of Quantum Dots. *Proc. Natl. Acad. Sci. USA* **2024**, *121*, e2307633121. [CrossRef]